Optical Fiber Technology xxx (xxxx) 102524

Contents lists available at ScienceDirect

Optical Fiber Technology

journal homepage: www.elsevier.com/locate/yofte

Regular Articles

# Saturable absorber based on the fiber coupler coated by CNTs

D.A. Stoliarov [a], P.A. Itrin [a], D.A. Korobko [a], V.A. Ribenek [a], L.V. Tabulina [b], A.V. Sysa [c], Yu.P. Shaman [c]

[a] Ulyanovsk State University, 42 Leo Tolstoy Str., 432017 Ulyanovsk, Russian Federation
[b] Belarusian State University of Informatics and Radioelectronics. 6, P.Brovka Str., 220013 Minsk, Belarus
[c] Scientific-Manufacturing Complex "Technological Centre", Shokin Sqr., 1, Zelenograd, 124498 Moscow, Russia

ARTICLE INFO

*Keywords:*
Fiber couplers
Saturable absorbers
Carbon nanotubes
Fiber ring lasers

ABSTRACT

We report on a new method for fabrication of saturable absorbers for operation in ring fiber lasers as a mode-locking element taking advantages of the manufacturing technologies of fiber couplers and microfiber tapers coated with carbon nanotubes. It is demonstrated in the experiment that the transmittance of the fabricated saturable absorber increases with an increase of the input radiation power. Also, we have shown that the fabricated saturable absorber enables generation of picosecond soliton pulses in ring fiber laser configuration.

## 1. Introduction

Currently, ultrashort pulse lasers are effectively used in various fields of everyday life. They are exploited both in research and services delivered to mass consumers, e.g., medicine, cosmetology, etc. Owing to a multiple consumer appeal, fiber lasers definitely benefit over all mode-locked lasers. Small size, relatively low cost, convenient fiber output, and high beam quality make them attractive for a large number of applications [1–6]. To deliver ultrashort pulses, a fiber laser configuration comprises either active [7] or passive mode–locking element with an incorporated saturable absorber. Low-cost and reliable passive mode-locking, mainly exploited in ultrashort pulse laser sources, enables generation of the pulses with a pulse duration much shorter than the modulator switching time [8].

Saturable absorbers (SA) are the key elements of passively mode-locked lasers. They conventionally could be divided in two types: artificial and natural SAs. Saturable absorbers based on Kerr lensing [9], nonlinear mirror [10], and nonlinear polarization rotation (NPR) belong to the first group [11,12]. NPR saturable absorbers are mainly used with fiber laser configurations. Although the lasers based on such SAs are easy-to-use, they are environmentally sensitive and require adjustment to initiate lasing that limits their practical application. Semiconductor mirrors (SESAM) [13,14] or SAs based on topological insulators [15], graphene [16], and carbon nanotubes (CNT) [17,18] belong to the group of natural SAs. Besides low cost and ease of use, the CNT technology is advantageous over the SESAM technology in ability to modulate transmittance thus simplifying laser circuits based on ring fiber cavities. As a result, CNT-based saturable absorbers have replaced SESAMs in a number of fiber laser applications [19–21].

The principle methods of CNT-based SAs fabrication are deposition of CNTs on a film, fiber end face [22,23], chemically etched d-shape fiber [24] or micro-taper obtained by thermal drawing of a standard fiber [25]. Each of the methods has specific limitations and drawbacks. In particular, the film method significantly limits the radiation power in the cavity [26], the d-shape technology requires special fiber structure and rather complicated [24]. In this work, we focus on the microfiber method of SA fabrication, in which CNTs are deposited on a fiber thermally drawn up to the diameters compared with the radiation mode area [25,27]. The evanescent field based CNT SA, manufactured by this method, has an advantage over the schemes using CNTs deposited on a film or fiber end face enabling generation of higher pulse energy and peak power. Such absorbers are simple to manufacture and easy-to-use, but suffer specific drawbacks. Due to a small diameter of taper waist region (~10 μm), when coated with CNTs at a high concentration or from a liquid phase, SA experiences high losses induced by the fiber deformation. The same restrictions impede the uniform distribution of CNTs over the microfiber surface. In addition, fiber tapers are sensitive to environment that can deteriorate their performance characteristics. To overcome these problems, the use of polymer composites has been proposed [28]. Along with additional protection of the microfiber, a polymer with a low refractive index (e.g., 2,2,2-trifluoroethyl methacrylate (PTFEMA), n = 1.42) provides the effective distribution of nanomaterial on its surface and prevents formation of agglomerations, thereby reducing SA losses from estimated 50% down to 15% [29,30].

In this work, we push forward development of the microfiber method for fabricating CNTs-based SAs. For this purpose, the fiber couplers commonly used in fiber circuits are employed. The fabrication process includes simultaneous thermal drawing of two parallel fibers

https://doi.org/10.1016/j.yofte.2021.102524
Received 17 November 2020; Received in revised form 3 March 2021; Accepted 3 March 2021

down to the diameters close to the mode field size followed by fusion [31]. The fibers fused into a coupler are elongated enough to enable interaction of radiation with the CNT film on their surface and saturable absorption. Since fiber coupler is a mechanically stronger structure than a standard microfiber, it is able to provide a simplified technology of CNT-film deposition in a polymer composition while maintaining a high saturation absorption coefficient. In particular, simplification of the technology within this approach allows using less precise (e.g., aerosol) methods of nanomaterial coating, which, in its turn, enables deposition of larger CNT-volumes and optimization of SA properties.

## 2. Manufacturing of a CNT-coated coupler

Single-walled CNTs (SWCNT) used for coupler coating have been synthesized by the electric arc technology at the Institute of Problems of Chemical Physics, the Russian Academy of Sciences (Chernogolovka, Russia). An average diameter of SWCNTs is 1.5 nm. Inset in Fig. 1 (a) shows the absorption spectrum of the used CNTs in the wavelength range 550–2400 nm. SWCNTs have been subjected to multistage liquid-phase treatment in order to obtain stable and homogeneous suspensions in a solution of 2,2,2-trifluoroethyl methacrylate (Sigma-Aldrich No. 373761) in N-methylpyrrolidone subsequently used as a matrix for SA structure [32]. Fig. 1 (a) shows the Raman spectra of the CNT structure before and after liquid-phase treatment. The spectra are obtained using LabRAM HR Evolution spectrometer at an exciting radiation wavelength of $\lambda_0$ =514 nm. The Raman spectrum analysis shows that CNTs demonstrate predominantly semiconductor conductivity [33]. Comparison of the intensities of spectrum lines D and G ($I_G/I_D$) gives estimations to the value $L_a$ describing the length of defect-free regions in the CNT structure [34,35]:

$$L_a(nm) = 2.4 \cdot 10^{-10} \lambda_0^4 \frac{I_G}{I_D} \quad (1)$$

The estimation shows that after a multi-stage liquid-phase treatment, the size of defect-free regions is reduced, on average from 504 nm down to 62 nm.

The 60/40 fiber coupler from the standard SMF fibers without cladding has been fabricated using the standard thermal fusion technology with a hydrogen torch for fiber couplers and WDM. The taper waist length, where the fiber cladding diameter decreases from 125 μm down to values close to the mode field diameter (9–10 μm), is $l = 18$mm. The intrinsic loss of the manufactured coupler is $L_0 = 0.5$ dB. Before coating with CNTs, the coupler is placed in a quartz cell and glued to keep its waist fixed in a suspended position. CNTs are deposited from the aerosol of the prepared suspension in a nitrogen atmosphere with infrared heating of the coupler surface up to 50° C. After a 10 min deposition, the CNTs cover almost the entire length of the coupler. (Fig. 1 (b)) and the coupling ratio has changed to 49/51 due to penetration of the CNT-polymer suspension into the coupler structure.

The image of the coupler waist region after CNT deposition taken by JEOL JSM-6010PLUS SEM is shown in Fig. 2 (a). Also, the coupler sample has been studied by the Raman spectroscopy methods. In Fig. 2 (b), the distribution of CNT G-band intensity (1570–1595 cm $^{-1}$) is shown in the coupler waist. The distribution is recorded under laser irradiation of the sample at the wavelength of 514 nm and power of 1 mW. The acquisition step and durations are 1 μm and 0.1 s, respectively. The blue color intensity is proportional to the G-band intensity that, in its turn, is proportional to a number of CNTs. The points corresponding to the minimal and maximal CNT G-band intensities are marked in Fig. 2 (b). One can see that CNT bundles are concentrated mainly in the trench between two tapered fibers forming the fused coupler.

## 3. Measurement of the saturable absorption

The key characteristic of a SA is the dependence of losses it introduces on the intensity (or power) of the input radiation. If the losses decrease with the input power, SA can be used for mode-locking and pulse generation through positive optical feedback in the laser cavity it provides [12].

A standard configuration shown in Fig. 3 (a) has been employed to evaluate characteristics of the fabricated CNT-coupler used as a saturable absorber [34,35]. A soliton laser operating at the wavelength of $\lambda = 1.55$ μm delivers pulses with the duration of ~1.4 ps and repetition rate of 3.84 MHz. A variable attenuator is used to control the power at the input of the manufactured CNT-coupler. Recording the power levels at all outputs of the experimental setup allows us to determine the transmittance of the CNT-coupler. The experimental results shown in Fig. 3 (b) describe the CNT - coupler transmittance as a function of the average power at the coupler input.

A change in the average power corresponds to a change in the peak power $P_0$ of the input soliton pulse (a simple estimation shows that 1 mW of the average power corresponds to $P_0 \approx 93$W). Therefore the same experimental results show the transmittance of the CNT - coupler as a function of the peak power at the coupler input. One can see a reliable increase of the coupler transmittance with an increase in the pulse peak power that is the key property of SA important for mode-locking. The experimentally measured depth of SA modulation is ~4.5%. However, the experimental data have been limited by the output power of the soliton source corresponding to its transition to the multipulse generation mode. Some theoretical estimations can be made using SA model with instantaneous relaxation time. In this model, the absorption coefficient $\alpha$ of SA, depending on the radiation power $P$, is expressed in terms of the modulation depth $\alpha_0$, saturation power $P_S$, and the value of unsaturated losses $\alpha_{NS}$:

$$\alpha = \frac{\alpha_0}{1 + P/P_s} + \alpha_{NS}$$

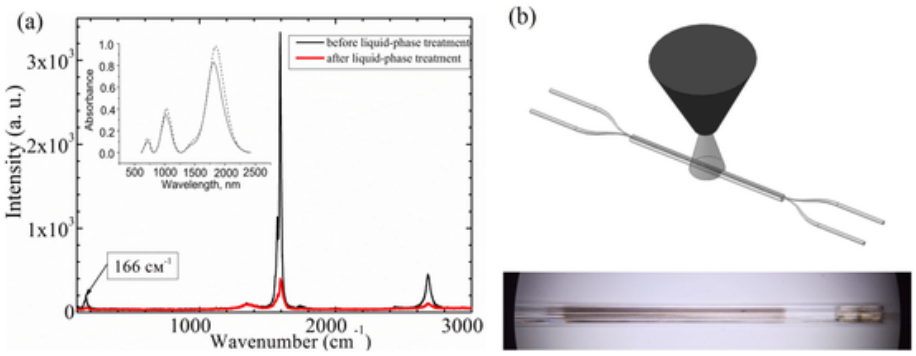


**Fig. 1.** (a) Raman spectra of the CNT structure before and after liquid-phase treatment. Inset: The CNTs absorption spectrum. (b) Schematic of CNT deposition on the fiber coupler surface and a photo of the fused fiber coupler covered by CNTs in a quartz cell.

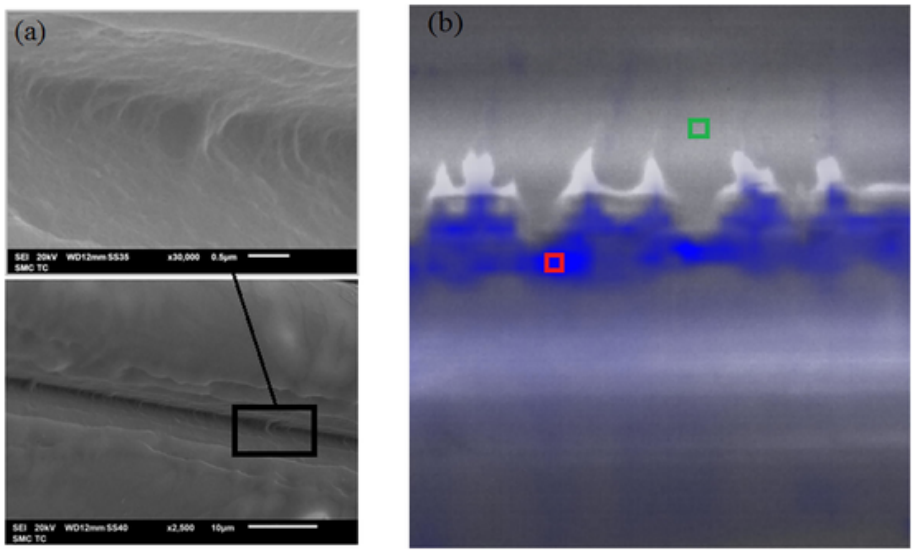


**Fig. 2.** (a) SEM image of CNTs located between optical fibers. (b) Image of the coupler irradiated at 514 nm to get the distribution of SWCNT G-band intensity. Red and green squares correspond to the maximum and minimum G + peak intensity (1590 $cm^{-1}$), respectively. (For interpretation of the references to color in this figure legend, the reader is referred to the web version of this article.)

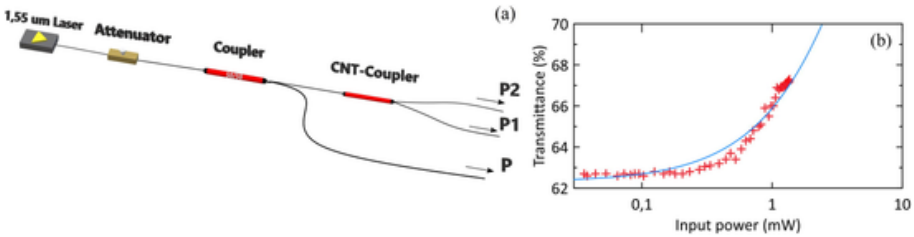


**Fig. 3.** (a) Schematic of the experimental setup for measuring saturable absorption in a CNT - coupler. (b) Experimentally measured coupler transmittance as a function of the radiation power at the input. Solid blue line is an approximation of the obtained data by dependence (2) for the parameters: $\alpha_0 = 18\%, P_S = 500Bm, \alpha_{NS} = 19\%$. (For interpretation of the references to color in this figure legend, the reader is referred to the web version of this article.)

For the soliton pulses with the sech$^2$ envelope and peak power $P_0$, the SA transmittance $T$ with instantaneous relaxation can be expressed through the parameter $s = P_0/P_S$ [35] as:

$$T = \frac{\alpha_0}{\sqrt{s(1+s)}} a\tanh\left(\sqrt{\frac{s}{1+s}}\right) + 1 - \alpha_{NS} \quad (2)$$

These estimations give the modulation depth of the fabricated SA $\alpha_0$>10% at high enough saturation power $P_S$>350W. Fig. 3 (b) shows an approximation for relation (2) at $\alpha_0 = 18\%, P_S = 500Bm, \alpha_{NS} = 19\%$.

## 4. Study of CNT-coupler in a ring fiber laser scheme

To study the mode-locking provided by the fabricated CNT - coupler, the coupler has been incorporated into a standard Er-doped fiber ring laser. The ring laser configuration (Fig. 4) contains no polarization-sensitive elements, so mode-locking through the nonlinear polarization rotation is prohibited in this scheme.

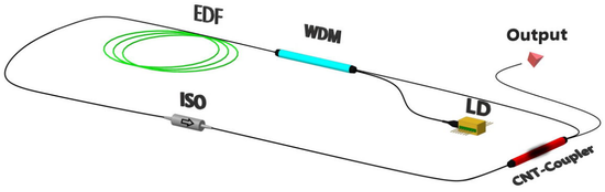


**Fig. 4.** Experimental set-up of a fiber laser with CNT- coupler. LD is the pump diode, WDM is the wavelength-division multiplexer, EDF is the Er-doped fiber, ISO is the fiber isolator.

The laser cavity contains 0.5 m of Er-doped EDF-150 fiber with a normal dispersion of 19 ps$^2$/km at 1550 nm. All other elements are connected by an SMF-28 fiber with a dispersion of –20 ps$^2$/km at 1550 nm. The total cavity length of 10.5 m corresponds to a fundamental repetition rate of 19.07 MHz, while the total cavity dispersion is ~ –0.196 ps$^2$. The configuration is pumped by a laser diode with a wavelength of 975 nm and a maximal power of 550 mW. The output radiation is emitted through a CNT- coupler. The laser self-starts to operate in a pulsed mode at a pump power of 50 mW, while the output power is 1.7 mW. The single-pulse lasing operation is maintained with the pump power levels up to 165 mW, whereas the output power increases to 3.3 mW. The optical spectrum and pulse autocorrelation describing this mode are shown in Fig. 5.

Despite an incomplete suppression of sidebands leading to a noticeable spectrum asymmetry, the pulse envelope shape is close to sech$^2$, while the product of the pulse duration (~7.2 ps) and pulse spectrum width (~0.4 nm) is TBW ~ 0.355, justifying that a pulse is close to a spectrally limited soliton. Fig. 6 shows the radiofrequency spectrum of the laser recorded with a resolution of 100 kHz. One can see that a stable spectrum comprising harmonics of the fundamental ring cavity mode exhibits no parasitic modulation and filtering. The signal-to-noise ratio for the fundamental (first-order) harmonic gets the level of >60 dB and then slowly decreases with the harmonic number thus highlighting a high quality of the laser signal.

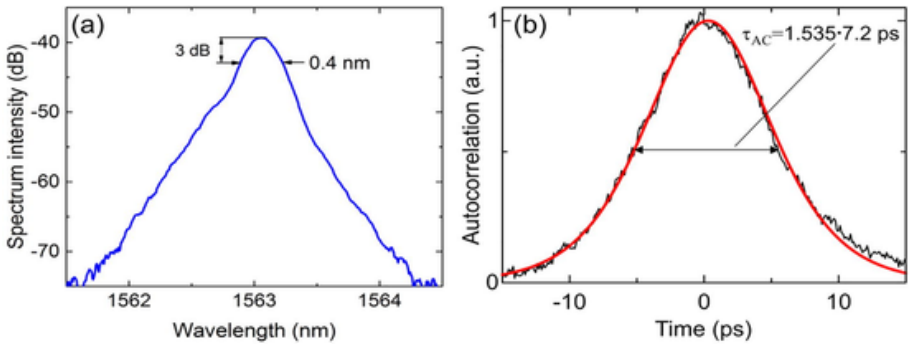


**Fig. 5.** (a) Optical spectrum and (b) autocorrelation of a laser pulse generated in mode-locked ring fiber laser with a CNT- coupler. The solid red line describes the $sech^2$ envelope. (For interpretation of the references to color in this figure legend, the reader is referred to the web version of this article.)

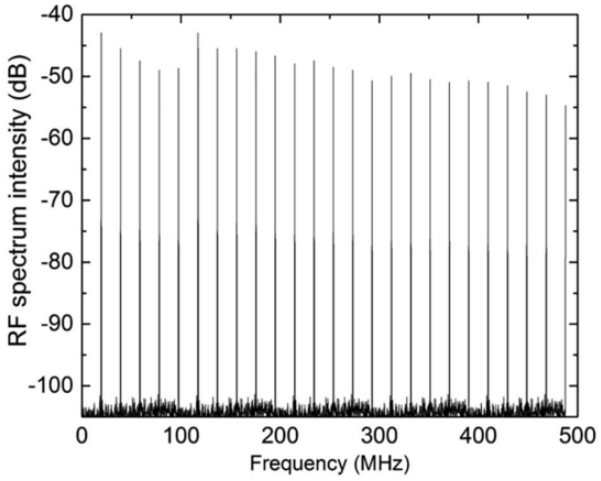


**Fig. 6.** Radiofrequency spectrum of mode-locked ring fiber laser with a CNT- coupler.

## 5. Conclusions

In this study, we propose a new fabrication method of SA for mode-locking of the ring fiber lasers taking advantages of the manufacturing technologies of fiber couplers and tapers coated with carbon nanotubes. The proposed method develops the technology of microfiber tapers coated with CNTs, but simplifying it, in particular, allowing usage of less complicated methods of nanomaterial deposition. The simplicity of the proposed CNT- coupler technology is in the use of widely available materials and standard laboratory equipment.

A standard experiment on measurement of the transmittance has confirmed that the fabricated sample of a CNT- coupler demonstrates the main property of SA, i.e. its transmittance increases with an increase in the peak power of the input pulse. The performed estimations show that this sample has a sufficiently high modulation depth (> 5%), however, its saturation power is also quite high ($P_S$>350W). Noteworthy, the use in the experiment of a pulsed source with the peak power of soliton pulses $P_0$<150W has not resulted in a change or degradation of the CNT- coupler characteristics.

The experiment has confirmed applicability of the CNT- coupler for mode-locking in a soliton ring fiber laser. In the reported laser configuration, the nonlinear polarization rotation effect on mode-locking is eliminated. The performance of the laser is not perfect, however, we have shown that the fabricated sample possesses the SA characteristics suitable for generation of picosecond soliton pulses. Specifically, the proposed technology is able to maintain generation of picosecond pulses in configurations with a relatively low Q-factor of the cavity (the output ratio of the used CNT- coupler is close to 50/50). In the future, the SA parameters will be further improved through the use of a CNT-coupler with lower output coefficients (10 or 5%) to increase the laser cavity Q-factor and generate pulses of much shorter duration. Also, we will upgrade the proposed technology using the improved SA characteristics (reduction of the saturation power and unsaturated losses), high quality CNTs fabrication and composition parameters (quantity, geometry) of nanomaterials. Promising methods of CNT deposition such as magnetron-sputtering-deposition method [36] and photonic crystal fiber assisted deposition [37] could be considered as more accurate and controllable fabrication process of CNT coated fiber couplers. We suppose that the optimizing device could be applied not only in the telecommunication range but also in other important spectral regions (for example, in 2 μm range)/

## Declaration of Competing Interest

The authors declare that they have no known competing financial interests or personal relationships that could have appeared to influence the work reported in this paper.

## Acknowledgments

This work was supported by the Russian Science Foundation (grant no. 19-72-10037) and the Ministry of Higher Education and Science of the Russian Federation (8th Megagrant Program, application # 2020-220-08-1369 and “State task #0830-2020-0009″).

## References

[1] W. Shi, Q. Fang, X. Zhu, R.A. Norwood, N. Peyghambarian, Fiber lasers and their applications, Appl. Opt. 53 (28) (2014) 6554–6568, https://doi.org/10.1364/AO.53.006554.
[2] M.E. Fermann, I. Hartl, Ultrafast fibre lasers. Nature photonics, 7 (11) (2013) 868-874. doi: 10.1038/nphoton.2013.280
[3] S. Droste, G. Ycas, B.R. Washburn, I. Coddington, N.R. Newbury, Optical frequency comb generation based on erbium fiber lasers, Nanophotonics 5 (2) (2016) 196–213, https://doi.org/10.1515/nanoph-2016-0019.
[4] U. Keller, Recent developments in compact ultrafast lasers, Nature 424 (6950) (2003) 831–838, https://doi.org/10.1038/nature01938.
[5] R.R. Gattass, E. Mazur, Femtosecond laser micromachining in transparent materials, Nat. Photonics 2 (4) (2008) 219–225, https://doi.org/10.1038/nphoton.2008.47.
[6] K. Wang, N.G. Horton, K. Charan, C. Xu, Advanced fiber soliton sources for nonlinear deep tissue imaging in biophotonics, IEEE J. Sel. Top. Quantum Electron. 20 (2) (2013) 50–60, https://doi.org/10.1109/JSTQE.2013.2276860.
[7] M. Bello-Jiménez, E. Hernández-Escobar, A. Camarillo-Avilés, O. Pottiez, A. Díez, M.V. Andrés, Actively mode-locked all-fiber laser by 5 MHz transmittance modulation of an acousto-optic tunable bandpass filter, Laser Phys. Lett. 15 (8) (2018) 85113, https://doi.org/10.1088/1612-202X/aac9d8.
[8] H.A. Haus, Mode-locking of lasers, IEEE J. Sel. Top. Quantum Electron. 6 (6) (2000) 1173–1185, https://doi.org/10.1109/2944.902165.
[9] T. Brabec, C. Spielmann, P.F. Curley, F. Krausz, Kerr lens mode locking, Opt. Lett. 17 (18) (1992) 1292–1294, https://doi.org/10.1364/ol.17.001292.
[10] F.Ö. Ilday, F.W. Wise, T. Sosnowski, High-energy femtosecond stretched-pulse fiber laser with a nonlinear optical loop mirror, Opt. Lett. 27 (17) (2002) 1531–1533, https://doi.org/10.1364/ol.27.001531.
[11] V.J. Matsas, T.P. Newson, D.J. Richardson, D.N. Payne, Self-starting,

passively mode-locked fibre ring soliton laser exploiting non-linear polarisation rotation, Electron. Lett. 28 (15) (1992) 1391–1393, https://doi.org/10.1049/el:19920885.
[12] C.J. Chen, P.K.A. Wai, C.R. Menyuk, Soliton fiber ring laser, Opt. Lett. 17 (6) (1992) 417–419, https://doi.org/10.1364/ol.17.000417.
[13] A. Isomaki, A.M. Vainionpaa, J. Lyytikainen, O.G. Okhotnikov, Semiconductor mirror for optical noise suppression and dynamic dispersion compensation, IEEE J. Quantum Electron. 39 (11) (2003) 1481–1485, https://doi.org/10.1109/JQE.2003.818285.
[14] O. Okhotnikov, A. Grudinin, M. Pessa, Ultra-fast fibre laser systems based on SESAM technology: new horizons and applications, New J. Phys. 6 (1) (2004) 177, https://doi.org/10.1088/1367-2630/6/1/177.
[15] C. Zhao, H. Zhang, X. Qi, Y.u. Chen, Z. Wang, S. Wen, D. Tang, Ultra-short pulse generation by a topological insulator based saturable absorber, Appl. Phys. Lett. 101 (21) (2012) 211106, https://doi.org/10.1063/1.4767919.
[16] Q. Bao, H. Zhang, Y.u. Wang, Z. Ni, Y. Yan, Z.X. Shen, K.P. Loh, D.Y. Tang, Atomic-layer graphene as a saturable absorber for ultrafast pulsed lasers, Adv. Funct. Mater. 19 (19) (2009) 3077–3083, https://doi.org/10.1002/adfm.v19:1910.1002/adfm.200901007.
[17] M. Chernysheva, A. Rozhin, Y. Fedotov, C. Mou, R. Arif, S.M. Kobtsev, S.K. Turitsyn, Carbon nanotubes for ultrafast fibre lasers. Nanophotonics, 6 (1) (2017) 1-30. doi: 10.1515/nanoph-2015-0156
[18] L. Huang, Y. Zhang, X. Liu, Dynamics of carbon nanotube-based mode-locking fiber lasers, Nanophotonics 9 (9) (2020) 2731–2761, https://doi.org/10.1515/nanoph-2020-0269.
[19] J. Wang, Y. Chen, W.J. Blau, Carbon nanotubes and nanotube composites for nonlinear optical devices, J. Mater. Chem. 19 (40) (2009) 7425–7443, https://doi.org/10.1039/b906294g.
[20] P. Avouris, M. Freitag, V. Perebeinos Carbon-nanotube photonics and optoelectronics. Nat. Photonics, 2 (6) (2008) 341-350. doi: 10.1038/nphoton.2008.94
[21] A. Martinez, Z. Sun, Nanotube and graphene saturable absorbers for fibre lasers, Nat. Photonics 7 (11) (2013) 842–845, https://doi.org/10.1038/nphoton.2013.304.
[22] A.I. Chernov, E.D. Obraztsova, A.S. Lobach, Optical properties of polymer films with embedded single-wall carbon nanotubes, Phys. Status Solidi (b) 244 (11) (2007) 4231–4235, https://doi.org/10.1002/pssb:200776152.
[23] M.A. Solodyankin, E.D. Obraztsova, A.S. Lobach, A.I. Chernov, A.V. Tausenev, V.I. Konov, E.M. Dianov, Mode-locked 1.93 μm thulium fiber laser with a carbon nanotube absorber, Opt. Lett. 33 (12) (2008) 1336–1338, https://doi.org/10.1364/ol.33.001336.
[24] D. Steinberg, J.D. Zapata, E.A.T. de Souza, L.A. Saito, Mechanically exfoliated graphite onto D-shaped optical fiber for femtosecond mode-locked erbium-doped fiber laser, J. Lightwave Technol. 36 (10) (2018) 1868–1874, https://doi.org/10.1364/JLT.36.001868.
[25] Z.C. Luo, M. Liu, H. Liu, X.W. Zheng, A.P. Luo, C.J. Zhao, W.C. Xu, 2 GHz passively harmonic mode-locked fiber laser by a microfiber-based topological insulator saturable absorber, Opt. Lett. 38 (24) (2013) 5212–5215, https://doi.org/10.1364/OL.38.005212.
[26] Y. Sui, V.J. Gokhale, O.A. Shenderova, G.E. McGuire, M. Rais-Zadeh, A thin-film infrared absorber using CNT/nanodiamond nanocomposite, MRS Online Proceedings Library 1452 (1) (2012) 8–13, https://doi.org/10.1557/opl.2012.1109.
[27] Y.-W. Song, K. Morimune, S.Y. Set, S. Yamashita, Polarization insensitive all-fiber mode-lockers functioned by carbon nanotubes deposited onto tapered fibers, Appl. Phys. Lett. 90 (2) (2007) 21101, https://doi.org/10.1063/1.2431445.
[28] K. Kieu, M. Mansuripur, Femtosecond laser pulse generation with a fiber taper embedded in carbon nanotube/polymer composite, Opt. Lett. 32 (15) (2007) 2242–2244, https://doi.org/10.1364/ol.32.002242.
[29] B. Xu, M. Omura, M. Takiguchi, A. Martinez, T. Ishigure, S. Yamashita, T. Kuga, Carbon nanotube/polymer composite coated tapered fiber for four wave mixing based wavelength conversion, Opt. Express 21 (3) (2013) 3651–3657, https://doi.org/10.1364/OE.21.003651.
[30] A. Martinez, M. Al Araimi, A. Dmitriev, P. Lutsyk, S. Li, C. Mou, A. Rozhin, M. Sumetsky, S. Turitsyn, Low-loss saturable absorbers based on tapered fibers embedded in carbon nanotube/polymer composites, APL Photonics 2 (12) (2017) 126103, https://doi.org/10.1063/1.4996918.
[31] G.P. Agrawal, Applications of nonlinear fiber optics, Academic press, 2020.
[32] V.A. Labunov, L.V. Tabulina, I.V. Komissarov, T.G. Rusal'skaya, I.A. Kashko, B.G. Shulitskii, Y.P. Shaman, E.P. Kitsyuk, A.V. Sysa, A.A. Polokhin, A.A. Pavlov, Effect of liquid-phase oxidative treatments on the purity, hydrophilicity, and structure of single-wall carbon nanotubes and on the electrical conductivity of their arrays, Russ. J. Appl. Chem. 93 (5) (2020) 679–690, https://doi.org/10.1134/S1070427220050080.
[33] H. Kataura, Y. Kumazawa, Y. Maniwa, I. Umezu, S. Suzuki, Y. Ohtsuka, Y. Achiba, Optical properties of single-wall carbon nanotubes, Synth. Met. 103 (1–3) (1999) 2555–2558, https://doi.org/10.1016/S0379-6779(98)00278-1.
[34] G. Sobon, A. Duzynska, M. Świniarski, J. Judek, J. Sotor, M. Zdrojek, CNT-based saturable absorbers with scalable modulation depth for Thulium-doped fiber lasers operating at 1.9 μm, Sci. Rep. 7 (2017) 45491, https://doi.org/10.1038/srep45491.
[35] C.C. Lee, J.M. Miller, T.R. Schibli, Doping-induced changes in the saturable absorption of monolayer graphene, Appl. Phys. B 108 (1) (2012) 129–135, https://doi.org/10.1007/s00340-012-5095-5.
[36] J. Wang, Z. Jiang, H. Chen, J. Li, J. Yin, J. Wang, T. He, P. Yan, S. Ruan, High energy soliton pulse generation by a magnetron-sputtering-deposition-grown MoTe 2 saturable absorber, Photonics Res. 6 (6) (2018) 535, https://doi.org/10.1364/PRJ.6.000535.
[37] J. Yin, F. Zhu, J. Lai, H. Chen, M. Zhang, J. Zhang, J. Wang, T. He, B.o. Zhang, J. Yuan, P. Yan, S. Ruan, Hafnium sulfide nanosheets for ultrafast photonic device, Adv. Opt. Mater. 7 (5) (2019) 1801303, https://doi.org/10.1002/adom.v7.510.1002/adom.201801303.